Magnetic MnAs nanoclusters in the diluted magnetic semiconductor $(Zn_{1-x}Mn_x)_3As_2$

1999 J. Phys.: Condens. Matter 11 8697

(http://iopscience.iop.org/0953-8984/11/44/308)

J. Phys.: Condens. Matter **11** (1999) 8697–8706. Printed in the UK PII: S0953-8984(99)03173-2

Magnetic MnAs nanoclusters in the diluted magnetic semiconductor $(Zn_{1-x}Mn_x)_3As_2$

R Laiho†, K G Lisunov†‡, E Lähderanta† and V S Zakhvalinskii†‡

† Wihuri Physical Laboratory, University of Turku, FIN-20014 Turku, Finland
‡ Institute of Applied Physics, Academiei str. 5, MD-2028 Kishinev, Moldova

Received 6 April 1999

Abstract. Magnetic properties of the II–V diluted magnetic semiconductor $(Zn_{1-x}Mn_x)_3As_2$ are investigated for $x = 0.08$, 0.10 and 0.13, between $T = 3$ and 500 K and in fields up to 60 kG. All samples show a steep decrease of the magnetization above 280 K. In low fields (5–80 G) the temperature dependence of the magnetic susceptibility is strongly irreversible below the blocking temperature $T_b \approx 250$ K. Above 15 kG the difference between the zero-field-cooled and the field-cooled susceptibilities disappears. These features give evidence for the presence of two magnetic subsystems: (i) paramagnetic centres including a single Mn ion and an open or closed triple antiferromagnetic cluster of Mn^{2+} and (ii) ferromagnetic MnAs nanoclusters. The size distribution of the MnAs clusters is described by two overlapping Gaussian functions with the maxima at $R_1 = 2.6$–3.1 nm and $R_2 = 3.3$–3.8 nm, depending on x.

1. Introduction

$(Zn_{1-x}Mn_x)_3As_2$, ZMA, is a derivative of Zn_3As_2 obtained by substitution of Mn for Zn. With x up to 0.135 it is isomorphic to Zn_3As_2 (so-called α-modification of Cd_3As_2, space group $I4_1cd$) [1]. ZMA belongs to a relatively new and less investigated family of the II–V group diluted magnetic semiconductors (DMSs) in which the Mn-alloyed II_3V_2 ternary and quaternary semiconductors [2] are the majority.

At temperatures higher than 100 K the magnetic properties of ZMA are determined by single Mn^{2+} ions [1]. When T is decreased a well measurable contribution from antiferromagnetic (AF) clusters of Mn^{2+} is observed with evidence for a spin-glass state below $T_f \sim 3$–4 K [1, 2]. Those investigations were made in relatively high magnetic fields. In low-field measurements a second spin-freezing effect was observed at temperatures as high as 200–250 K in ZMA with $x = 0.08$–0.13, provided that the field was less than 100 G [3–5]. The coexistence of two spin-glass-like states, one at high and another at low temperatures, has been found also in $Cd_{1-x-y}Mn_xFe_yTe$ with $x = 0.37$ and $y = 0.01$ [6]. Different mechanisms have been proposed for explanation of the high-temperature spin freezing in these DMSs [5–7], without still reaching a fully conclusive picture. On the other hand, irreversible behaviour of the susceptibility and magnetic freezing observed at $T \sim 250$ K in $Zn_{1-x}Mn_xAs_2$ were attributed to ferromagnetic (FM) MnAs nanoclusters [8].

In this paper we report investigations of the magnetic properties of $(Zn_{1-x}Mn_x)_3As_2$ with $x = 0.08$–0.13. Using specimens with a relatively high Mn concentration we expect to obtain information about the presence and nature of MnAs clusters in this material. The contribution of different clusters to the high-temperature magnetic freezing phenomena is discussed.

0953-8984/99/448697+10$30.00

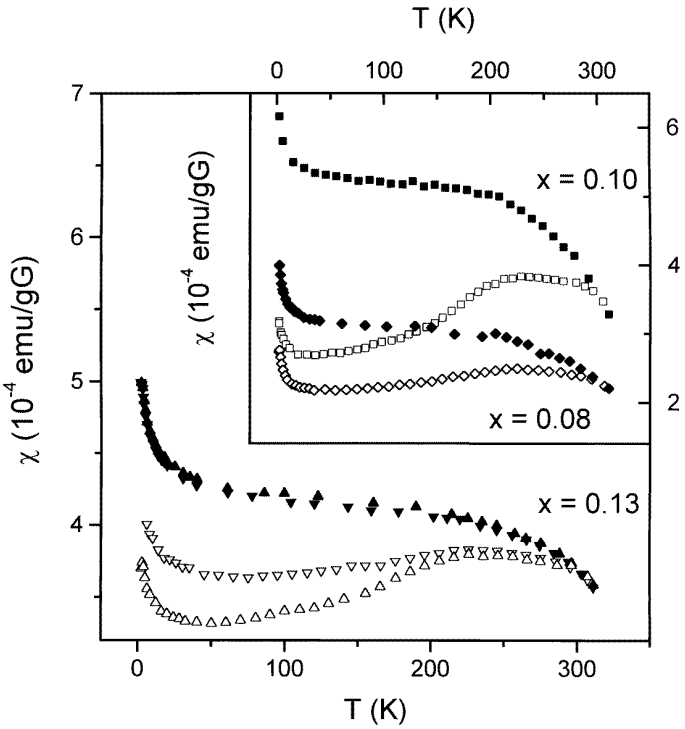

Figure 1. Temperature dependences of χ_{ZFC} (open symbols) and χ_{FC} (closed symbols) for ZMA with $x = 0.13$ measured in the field of $B = 10$ G (Δ) and 80 G (∇). Inset: $\chi_{ZFC}(T)$ and $\chi_{FC}(T)$ for ZMA with $x = 0.08$ and $B = 10$ G, and $x = 0.10$ and $B = 5$ G.

2. Experimental results

Single crystals of ZMA with $x = 0.08$, 0.10 and 0.13 were grown by the modified Bridgman method (slow cooling of a melt in the presence of a temperature gradient in a furnace) [3]. Details of the preparation and characterization of the specimens (structure, composition and homogeneity) are described in [3]. Dc magnetic measurements were made separately between 3–310 K and 250–500 K with a SQUID magnetometer extending considerably the temperature range (5–220 K) attainable in our previous experiments [3, 4]. Before every measurement the sample was annealed for 0.5–2 h at a temperature between 150 and 200 °C to remove traces of any possible remanent magnetization.

The temperature dependence of the magnetization, $M(T)$, was measured after cooling the sample in zero ($B < 0.1$ G) field (ZFC) or while cooling it in a field (FC). As can be seen from figure 1 the plots of $\chi_{ZFC}(T)$ and $\chi_{FC}(T)$ ($\chi = M/B$) measured in fields of $B = 5$–10 G deviate from one another below $T_i \approx 280$ K and $\chi_{ZFC}(T)$ has a broad maximum around $T_b \approx 250$ K. The difference between $\chi_{ZFC}(T)$ and $\chi_{FC}(T)$ decreases strongly on increasing the measuring field and disappears completely at $B = 15$ kG (figure 2(a)). The magnetic properties described above reproduce well the previous results for ZMA with $x = 0.08$–0.13, obtained in the temperature region below 220 K [3, 4]. Additionally, as evident from figure 2(b), the magnetization curve $M(B)$ observed at $T = 3.3$ K starts to deviate from linearity already in fields above a few kilogauss.

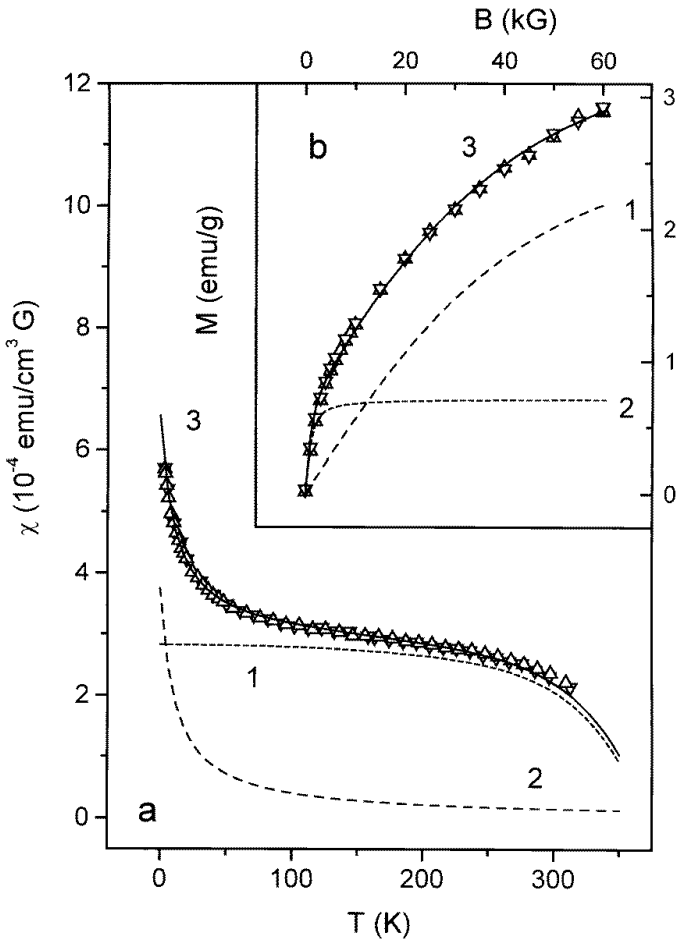

Figure 2. (a) Temperature dependence of χ_{ZFC} (Δ) and χ_{FC} (∇) for ZMA with $x = 0.13$ and $B = 15$ kG. Lines 1 and 2 represent the contributions of the first and the second term of $\chi(T)$ in equation (6), respectively, and line 3 is their sum. (b) Magnetic field dependence of the magnetization for $x = 0.13$ at $T = 3.3$ K measured in an increasing (Δ) and decreasing (∇) magnetic field. Lines 1 and 2 show the contributions of the first and the second term of $M(B)$ in equation (7), respectively, and line 3 is their sum.

A completely new result is shown in figure 3: above $T_i \approx 280$ K the functions $\chi_{ZFC}(T)$ and $\chi_{FC}(T)$ fall together and above 350 K the susceptibility approaches a constant value which is small in comparison with that observed at T_i.

3. Discussion

The magnetic properties of ZMA described above give strong evidence for the presence of FM MnAs nanoclusters in all the samples investigated. The structure of bulk MnAs is hexagonal $B8_1$ (NiAs type) above $T_D = 394$ K and orthorhombic $B31$ (MnP type) below T_D [9]. These phases are paramagnetic (PM) [9]. On cooling in zero field a first-order magnetostructural phase transition takes place at $T_{Cc} \approx 306$ K, again to a hexagonal $B8_1$ modification with a

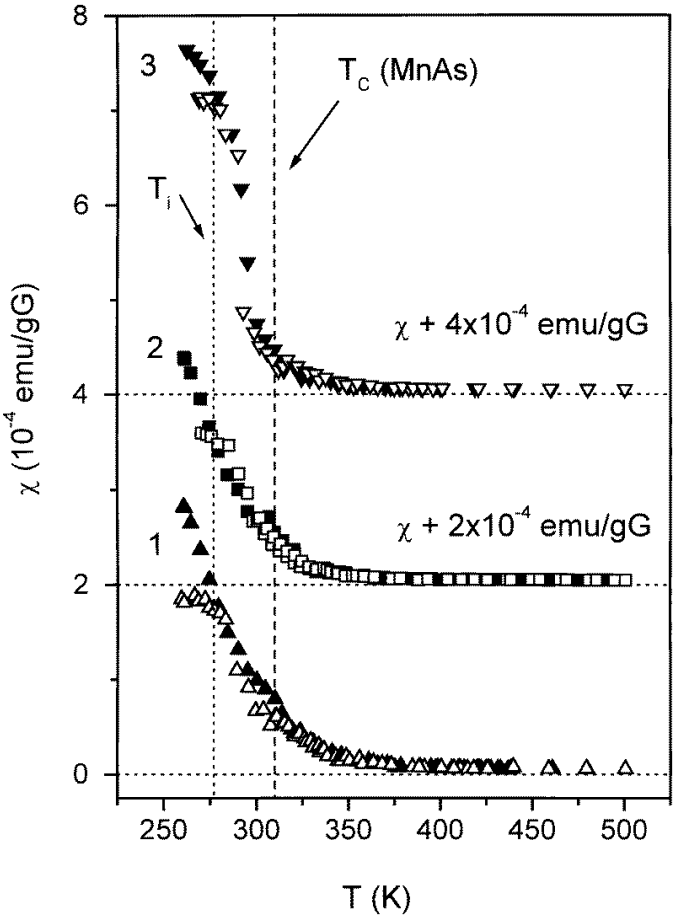

Figure 3. Temperature dependence of χ for ZMA with $x = 0.08$ (1), 0.10 (2) and 0.13 (3), measured in the field of $B = 80$ G. The open and closed symbols represent χ_{ZFC} and χ_{FC}, respectively. The dashed and the dotted lines give the Curie temperature T_C of MnAs and the temperature of the onset of irreversibility, T_i, respectively. For convenience the plots (2) and (3) are shifted along the χ axis by the amount shown above the corresponding curves.

spontaneous magnetization $\sigma_s(T)$. On heating in zero field σ_s vanishes at $T_{Ch} \approx 317$ K [9]. The FM-like transition temperatures, T_C, of the investigated ZMA samples are close to the average of T_{Cc} and T_{Ch} given by the vertical dashed line in figure 3. The steep decrease of the magnetization just below $T_C \approx 310$ K, indicating the presence of MnAs clusters, has been observed earlier in the III–V DMS $In_{0.82}Mn_{0.18}As$ [10] and in the II–V_2 DMS $Zn_{1-x}Mn_xAs_2$ with $x = 0.01$–0.1 [8].

Generally, small single domain FM particles incorporated in a solid matrix can exist in two different states [11]. At temperatures above the blocking temperature T_b thermal fluctuations can cause a sort of Brownian rotation of the magnetic moment of the particles with the result that an assembly of such particles exhibits superparamagnetic (SP) behaviour. In this case the magnetization of the FM clusters having the volume V and the magnetic moment $\mu = \sigma_s V$

satisfies the equation

$$M_{FM} = M^*_{FM} L(\mu B/k_B T) \tag{1}$$

where $M^*_{FM} = \eta\sigma_s$ is the saturation magnetization of the assembly of the FM particles with the volume fraction η and $L(\xi)$ is the Langevin function. At $T < T_b$ the moments of the particles are blocked, with their directions distributed in random over the sample volume. There are two conceivable sources of the blocking barriers: (i) the anisotropy energy of individual particles and (ii) the dipolar interaction between the moments of different particles.

In case (i) the moment of each particle is stabilized independently when its anisotropy energy, KV, becomes high enough to counteract the thermal excitations having the energy $\sim k_B T$. Here K is the density of the anisotropy energy and V is the volume of the particle. After removal of the external field the moments of the particles relax towards an equilibrium state. The relaxation time, τ, is given by $1/\tau = f_0 \exp(-KV/k_B T)$, where f_0 is a frequency factor of the order of 10^9 s^{-1} [11]. If a plausible value of $\tau = 10^2$ s is used as the criterion for transition to stable behaviour the energy barrier is $25\,k_B T$. Then the blocking temperature can be written as [11]

$$T_b^{(anis)} = KV/25\,k_B. \tag{2}$$

In case (ii) the blocking temperature and the magnetization for $T < T_b$ will satisfy the equations [8]

$$T_b^{(inter)} = \mu^2 I_0^{1/2}/3\,k_B \tag{3}$$

and

$$M_{FM} = M^*_{FM} B/(B + \xi M_s) \tag{4}$$

respectively. The saturation magnetization in equation (4) can be written as $M^*_{FM} = \mu N$ where N is the concentration of the particles. In equations (3) and (4) we have $I_0 = z_I/r^6$ where $z_I = 11.6$ and $r = 2(4\pi N/3)^{-1/3}$ is the mean distance between the particles, and $\xi = 17.3$ [8].

The blocking transition (i.e. transition from the SP to stable behaviour) of an assembly of single-domain particles can be identified by deviation of $\chi_{ZFC}(T)$ from $\chi_{FC}(T)$. The blocking temperature T_b is defined by the cusp in $\chi_{ZFC}(T)$ meaning that for $T > T_b$ the thermal energy is large enough to enable the clusters to be oriented by an external magnetic field. Below T_b the clusters cannot overcome the blocking barriers (independent of their nature) [11] with the help of thermal excitations. Blocking temperatures as high as the room temperature have been established e.g. in heterogeneous metallic Cu–Co alloy films containing nanometre scale FM Co-rich clusters [12] and in the III–V semiconductor GaAs with Fe_3GaAs precipitates [13]. Lower values of T_b were observed in some granular systems demonstrating the SP response of the clusters and related giant magnetoresistance (see [13] and references therein). Accordingly, the high-temperature irreversible phenomena shown in figure 1 can be attributed to the presence and blocking of the FM MnAs cluster moments in the samples. The broad maximum of $\chi_{ZFC}(T)$ suggests a distribution of the blocking temperatures around $T_b \approx 250$ K and, as follows from equation (2), a distribution of the sizes of the FM clusters.

Taking into account the proximity of the temperatures T_i and T_C and the relation $M(T_i) \gg M(T)$ at $T > T_C$ (figure 3), the volume fraction of MnAs in ZMA can be determined from the equation

$$\eta \approx \frac{M(T_i)\rho_{ZMA}}{\sigma_s(T_i)\rho^L_{MA}[25\sigma_s(T_i)B/K(T_i)]} \tag{5}$$

where $\rho_{MA} = 6.25$ g cm^{-3} and $\rho_{ZMA} = \rho_{ZA}\mu_{ZMA}/\mu_{ZA}$ are the mass densities of MnAs and ZMA (here $\rho_{ZA} = 5.60$ g cm^{-3} is the density of Zn_3As_2 and μ_{ZMA}, μ_{ZA} and μ_{MA} are

the molecular weights of ZMA, Zn_3As_2 and MnAs, respectively). At $T_i = 280$ K we have $\sigma_s(T_i) \approx 115$ emu g^{-1} and $K(T_i) \approx 8 \times 10^6$ erg cm^{-3} [14] which gives $\eta \approx 2.3 \times 10^{-3}$, 3.5×10^{-3} and 3.8×10^{-3} for ZMA with $x = 0.08$, 0.10 and 0.13, respectively. These values of η correspond to the fraction of Mn ions entering the FM clusters, $\beta = \rho_{MA}\mu_{ZA}\eta/(\rho_{ZA}\mu_{MA}x)$, as $\beta \approx 0.086$, 0.10 and 0.087 and those of $x^* = x(1-\beta) \approx 0.07$, 0.09 and 0.12 in the rest of the material for $x = 0.08$, 0.10 and 0.13, respectively. Hence, in ZMA only a small part of the Mn ions is bound in the FM clusters, in comparison with $Zn_{1-x}Mn_xAs_2$ where the values of $\eta = (2.3\text{–}3.5) \times 10^{-2}$ and $\beta = 0.97\text{–}0.73$ for $x = 0.05\text{–}0.10$ are much higher [8]. On the other hand, opposite to $Zn_{1-x}Mn_xAs_2$, in ZMA both $\chi_{ZFC}(T)$ and $\chi_{FC}(T)$ increase rapidly when T is decreased below ~30 K (figure 1). From comparison of the values of η and β in ZMA and in $Zn_{1-x}Mn_xAs_2$ we can conclude that in ZMA the majority of the Mn ions outside the FM MnAs clusters can form paramagnetic (PM) centres explaining the increase of $\chi_{ZFC}(T)$ and $\chi_{FC}(T)$ at low temperatures (figure 1).

To determine the nature of the PM centres, first we analyse the temperature dependence of the susceptibility in figure 2(a). Taking into account the disappearance of the irreversibility of $\chi(T)$ at $B = 15$ kG and assuming a linear response of the PM centres to the applied field, we fit $\chi(T)$ in figure 2(a) with the equation

$$\chi(T) = \eta\frac{\sigma_s(T)}{B} + \frac{C}{T-\theta} \tag{6}$$

where the first term represents the contribution from FM MnAs clusters. The diamagnetic background of the host material Zn_3As_2, $\chi_0 = -0.12 \times 10^{-5}$ emu cm^{-3} G [3], is small and can be neglected. If outside the FM clusters in ZMA all Mn^{2+} formed only the single ion PM centres, the second term in equation (6) would describe exactly the PM contribution, with the Curie constant $C = p_{eff}^2\mu_B^2N_0x^*/3k_B$ where p_{eff} is the effective number of the Bohr magnetons, μ_B per Mn ion, N_0x^* is the concentration of Mn in ZMA outside FM clusters and θ is the Curie–Weiss temperature introduced to account for the interaction between the Mn ions. The dependence of σ_s on T is given in [14]. The function $\chi(T)$ evaluated with equation (6) is shown by the solid line in figure 2(a). The contributions of the first and the second terms in the right-hand side of equation (6) are displayed by the dotted and the dashed lines, respectively. From the best fit with equation (6) we obtain $C = (420 \pm 30) \times 10^{-5}$ emu cm^{-3} G K^{-1}, $\theta = -10.7 \pm 0.8$ K and $\eta = (4.3 \pm 0.4) \times 10^{-3}$. The value of η agrees well with that found above with equation (5) for the sample with $x = 0.13$. However, the value of $p_{eff}^2 \approx 5.9$ calculated from C is much smaller than the effective number of the Bohr magnetons for free Mn^{2+} ($p_{eff}^2 = 35$) or for single Mn ions in ZMA with $x = 0.005\text{–}0.049$ ($p_{eff}^2 \approx 29\text{–}26$, respectively) [1]. The interaction between single Mn ions in ZMA is described by the function $\Theta(x) \approx -(2000 \pm 200)x$ (in K) [1], which for $x = 0.12\text{–}0.13$ exceeds considerably the Curie–Weiss temperature $\theta = -10.7$ K found above. These disagreements point out that outside the FM nanoparticles Mn ions exist not only in the single ion state but can form also small clusters with strong AF interaction between ions inside the clusters. Such AF clusters have been found in many other Mn-based DMSs [15] as well as in the II–V group materials when Mn concentration is increased [1, 2].

Important information about the AF clusters in ZMA can be obtained by fitting the magnetic field dependence of the low-temperature magnetization data shown in figure 2(b) with the equation

$$M(B) = M_{PM}(B) + M_{FM}(B). \tag{7}$$

The contribution of the PM centres to equation (7) can be expressed with a phenomenological equation [15] $M_{PM}(B) = M_{PM}^* B_{5/2}[5\mu_B B/k_B(T+T_0)]$ where $M_{PM}^* = \mu_B g S_0 N_0 x^*$, gS_0 and T_0 are the effective spin per Mn ion and the effective temperature, respectively, and $B_{5/2}(\xi)$

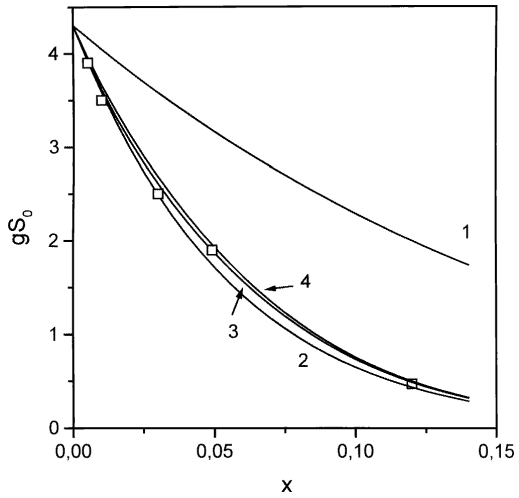

Figure 4. gS_0 against x in ZMA (open squares) obtained in [1] ($0.0052 \leqslant x \leqslant 0.049$) and in this work ($x^* = 0.12$). The lines 1–4 are calculated as described in the text.

is the Brillouin function. As evident from figure 2(b) no difference between the curves $M(B)$ obtained by increasing or decreasing the magnetic field is observed at $T = 3.3$ K up to $B = 60$ kG. That is why the contribution to the net magnetization from the FM clusters (the second term in equation (7)) in a sufficiently strong field is determined by reversible processes. Therefore, using equations (1) and (2) and neglecting the size distribution of the FM clusters we obtain $M_{FM}(B) \approx \eta\sigma_s L(25\sigma_s B/K)$. The dependence $M(B)$ calculated with equation (7) is shown by the solid line in figure 2(b). The contributions of the first and the second term to equation (7) are given by the dashed and the dotted lines, respectively (in calculations we use the low-temperature values of $\sigma_s \approx 144$ emu g^{-1} and $K \approx 12 \times 10^6$ erg cm^{-3} [14]). From the best fit with equation (7) we obtain $\eta = (4.5 \pm 0.5) \times 10^{-3}$, $T_0 = 3.5 \pm 0.5$ K and $gS_0 = 0.47 \pm 0.01$.

The value of η agrees with those obtained from equations (5) and (6) and T_0 is comparable with the corresponding values found in other DMSs. On the other hand, gS_0 is an order of magnitude lower than for free Mn^{2+} ($gS = 5$) or for single Mn ions in ZMA with $x = 0.0052$–0.049, $gS_0^* = 4.3 \pm 0.2$ [1]. The effective spin per Mn ion can be expressed in the form [15]

$$gS_0 = gS_0^*(P_1 + P_{O3}/3 + P_{C3}/15 + \cdots) \tag{8}$$

where the terms in the parenthesis represent probabilities of Mn^{2+} to be in the single ion state (P_1), in the open (P_{O3}) or closed (P_{C3}) triples or in the larger AF clusters (...). These probabilities can be expressed as different polynomial functions of x depending on the type of the crystal lattice and the number of interactions between Mn ions taken into account [15, 16]. The metallic atoms in the lattice of ZMA occupy the sites of a slightly distorted cube [2]. Therefore, we calculated gS_0 using the corresponding expressions in [16] obtained for the sc lattice. In figure 4 is presented the function $gS_0(x)$ evaluated by taking into account only single ion centres and interactions between only nearest neighbours (line 1). In this figure are shown also the dependences of gS_0 on x, calculated by taking into account interactions between both the nearest and next-nearest neighbours for singles (line 2), singles and open triples (line 3) and singles and open and closed triples (line 4). These dependences are compared

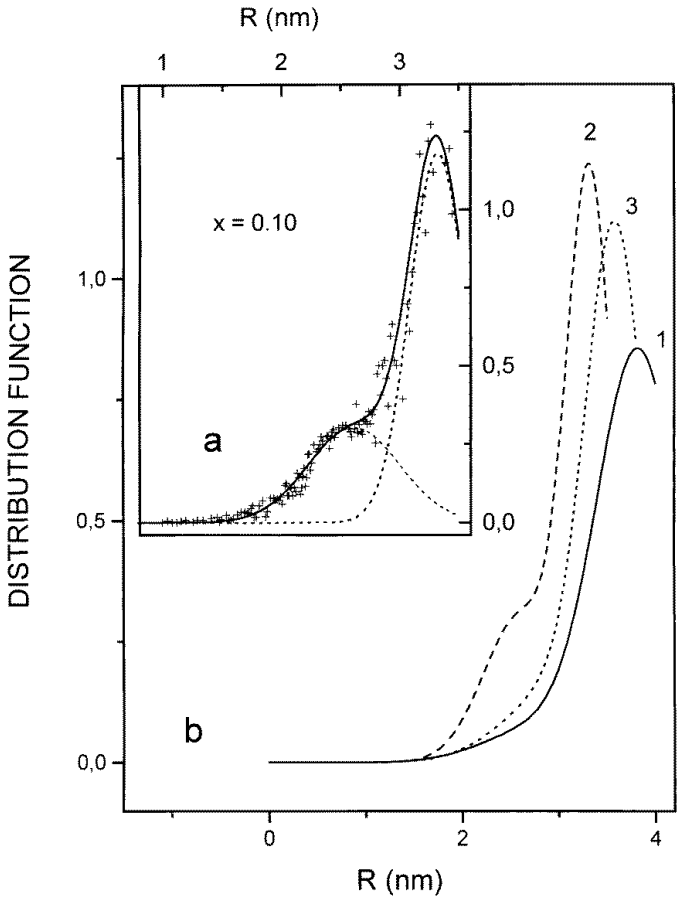

Figure 5. Expression of the distribution function of the FM cluster radius R in ZMA with $x = 0.10$ (+) by two overlapping Gaussian functions (a) and the distribution functions for the samples with $x = 0.08$ (line 1), 0.10 (line 2) and 0.13 (line 3) (b).

with the experimental values of gS_0 obtained in this work for $x^* \approx 0.12$ and in [1]. In [1] the analysis of the magnetization was performed neglecting the contribution of the FM clusters. This assumption is justified in ZMA only below $x \approx 0.05$ (where the difference between $\chi_{ZFC}(T)$ and $\chi_{FC}(T)$ disappears [3]). Therefore, from [1] we chose only the data obtained for x between 0.0052 and 0.049. As evident from figure 4, for $x \leqslant 0.03$ the PM response of ZMA is governed by single ion centres (line 2) when the interactions are extended to the nearest and next-nearest neighbours. Above $x = 0.03$ some contribution from the triples (see line 3) of Mn ions interacting with the nearest and next-nearest neighbours does exist also. No influence of the AF clusters larger than triples can be observed up to $x \approx 0.12$. Comparing with the II–VI group Mn-based DMSs, the influence of larger clusters is observed in these materials starting from $x \approx 0.05$–0.06 [15]. A possible reason for this difference may be presence of FM nanoclusters in ZMA and the gradual growth of their fraction when the total concentration of Mn is increased above $x \approx 0.05$, which does not take place in the II–VI group DMSs.

As mentioned above, the broad maximum of $\chi_{ZFC}(T)$ suggests a distribution of the blocking temperature around $T_b \approx 250$ K, corresponding to the distribution of the sizes of

the FM clusters. The distribution function of the blocking temperature can be evaluated with the equation [8, 16]

$$F(T) = \frac{1}{\gamma}\frac{\mathrm{d}}{\mathrm{d}T}\left[\frac{T\chi_{ZFC}(T)}{\sigma_s^2(T)}\right] - \lambda. \tag{9}$$

The distribution function, $f(R)$, of the cluster radius, R (or the radius of a sphere of equivalent volume) is calculated using equation (2) and the temperature dependences of K and σ_s [14]. The constants λ and γ are determined by normalizing $f(R)$ to unity and using the condition $f(R) = 0$ at $R = 0$. As evident from figure 5(a) the normalized distribution function for ZMA with $x = 0.10$ has a sharp peak at $R_1 \approx 3.3$ nm. Analysis of $f(R)$ using two Gaussian functions reveals another peak at $R_2 \approx 2.6$ nm. For the specimens with $x = 0.08$ and 0.13 the distribution functions in figure 5(b) are also described by two overlapping Gaussians (only their sum is shown), with the peaks at $R_1 \approx 3.8$ nm and 3.6 nm and at $R_2 \approx 2.8$ nm and 3.1 nm, respectively. These values are similar to the sizes of FM clusters in $Zn_{1-x}Mn_xAs_2$, excluding the somewhat lower values of R_1 and R_2 (3.3 and 2.4 nm, respectively) and the contribution of an additional Gaussian with a weak peak at $R_3 \approx 1.7$ nm [8]. This suggests that the mechanisms of generating the FM MnAs nanoparticles in these materials are similar.

The above discussion gives sufficient evidence that the contribution of the FM MnAs clusters to the net magnetization of ZMA is governed by local anisotropy fields acting on the spins inside each cluster (the first out of the two sources of the blocking barriers mentioned above). In $Zn_{1-x}Mn_xAs_2$ the moments of the FM clusters are blocked by the same mechanism [8]. This can be demonstrated independently by comparing the scales of the anisotropy energy, W_a, and the energy of the dipolar interaction, W_d, if the latter is assumed to be predominant in formation of the blocking barriers. By fitting the magnetization in figure 2(b) with equation (7) where $M_{FM}(B)$ is given by equation (4) we obtain $M^*_{FM} \approx 5.2$ emu cm^{-3}, $gS_0 \approx 0.47$ and $T_0 \approx 5.1$ K. Using equation (3), the relation $M^*_{FM} = \mu N$ and the values of $T_b \approx 250$ K and $M^*_{FM} \approx 5.2$ emu cm^{-3} we find the following typical values of the moment and the concentration of the FM clusters (if their size distribution is neglected): $\mu \approx 1.2 \times 10^6\,\mu_B$ and $N \approx 4.6 \times 10^{14}$ cm^{-3}. Using these values, we obtain $V = M^*_{FM}/\sigma_s N \approx 1.3 \times 10^{-17}$ cm^3, $r = 2(4\pi N/3)^{-1/3} \approx 1.6 \times 10^{-5}$ cm, $W_a = KV \approx 95$ eV and $W_d = z_J\mu^2/r^3 \approx 0.6$ eV. The value of $W_a \gg W_d$ contradicts the assumption made above that our magnetization data can be explained by attributing the blocking of the cluster moments to the dipolar interaction.

4. Conclusions

In this work magnetic properties of ZMA are investigated for $x = 0.08$, 0.10 and 0.13. The dependences of the magnetization on the temperature and magnetic field give evidence for the presence of two magnetic subsystems, PM centres and FM MnAs nanoclusters, in this material. The former subsystem consists presumably of single Mn ions with some admixture of open or closed triple AF clusters of Mn^{2+}. No influence to the PM response from the AF clusters larger than triples is observed up to $x \approx 0.12$. Clear irreversible phenomena are observed in low magnetic fields, reflecting a blocking transition in the dynamics of the magnetic moments of the FM clusters about 10% below the ferromagnetic Curie temperature of bulk MnAs. The size distribution of the MnAs clusters in ZMA is found to be similar with that of $Zn_{1-x}Mn_xAs_2$ [8], suggesting that the mechanism of generation of the MnAs nanoparticles is similar in both materials. On the other hand, the volume fraction of MnAs is an order of magnitude smaller in ZMA than in $Zn_{1-x}Mn_xAs_2$. Because both materials are obtained with the same crystal growth method, a likely reason is the difference of the lattice structures of ZMA (α-Cd_3As_2 type, space group $I4_1cd$) and $Zn_{1-x}Mn_xAs_2$ (β-ZnP_2 type, space group $P2_1/c$).

References

[1] Denissen C J M, Sun Dakun, Kopinga K and de Jonge W J M 1987 *Phys. Rev.* B **36** 5316
[2] Cisowski J 1997 *Phys. Status Solidi* b **200** 311
[3] Lashkul A V, Lähderanta E, Laiho R and Zakhvalinskii V S 1992 *Phys. Rev.* B **46** 6251
[4] Lähderanta E, Laiho R, Lashkul A, Zakhvalinskii V, Roy S B and Caplin A D 1992 *J. Magn. Magn. Mater.* **104–107** 1605
[5] Chudinov S M, Kulbachinski V A, Svistunov I V, Mancini G and Davoli I 1992 *Solid State Commun.* **84** 531
[6] Irie Y, Sato T and Ohta E 1995 *Phys. Rev.* B **51** 13 084
[7] Laiho R, Lashkul A V, Lähderanta E, Lisunov K G, Stamov V N and Zakhvalinskii V S 1995 *J. Phys.: Condens. Matter* **7** 7629
[8] Laiho R, Lisunov K G, Lähderanta E and Zakhvalinskii V S 1999 *J. Phys.: Condens. Matter* **11** 555
[9] Pytlik L and Zieba A 1985 *J. Magn. Magn. Mater.* **51** 199
[10] Ohto H, Munekata H, von Molnar S and Chang L L 1991 *J. Appl. Phys.* **69** 6103
[11] Bean C P and Livingston J D 1959 *J. Appl. Phys.* **30** 120S
[12] Berkowitz A E, Mitchell J R, Carey M J, Young A P, Rao D, Starr A, Zhang S, Spada F E, Parker F T, Hutten A and Thomas G 1993 *J. Appl. Phys.* **73** 5320
[13] Pekarek T M, Crooker B C, Nolte D D, Deak J, McElfresh M, Chang J C P, Harmon E S, Melloch M R and Woodal J M 1997 *J. Magn. Magn. Mater.* **169** 261
[14] De Blois R W and Rodbell D S 1963 *J. Appl. Phys.* **34** 1101
[15] Oseroff S and Keesom P H 1988 *Semiconductors and Semimetals* vol 25 (London: Academic) p 73
[16] Kreitman M M and Barnett D L 1965 *Phys. Rev.* **43** 364